



# Adsorption of the crystal violet dye on an adsorbent material prepared from Moroccan oil shales

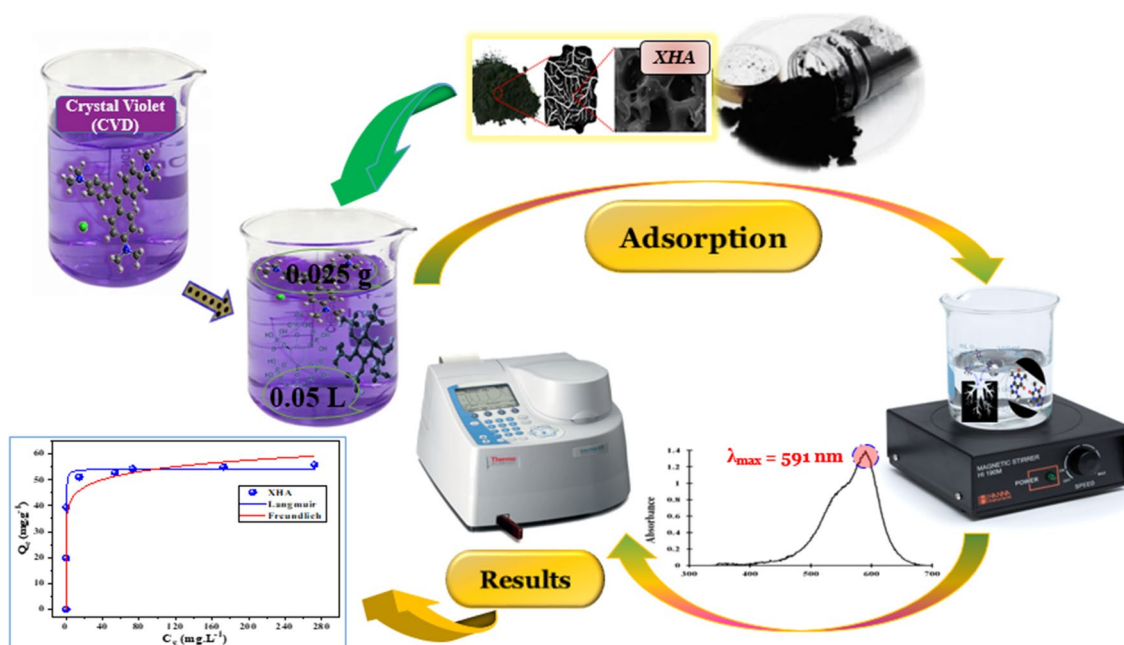
E. H. Chafyq<sup>1</sup> · K. Legrouri<sup>1,2</sup> · M. Aghrouch<sup>4</sup> · M. Oumam<sup>1</sup> · S. Mansouri<sup>3</sup> · E. Khouya<sup>1,5</sup> · H. Hannache<sup>1,3</sup>

Received: 14 May 2022 / Accepted: 4 September 2022 / Published online: 20 September 2022  
© Iranian Chemical Society 2022

## Abstract

The aim of this work was the elaboration and characterization of materials prepared from the Moroccan oil shales of the Timahdit region (layer X) and their use for the removal of the crystal violet dye from aqueous solutions. The adsorbent material, referred to as XHA, was characterized by several analytical and spectroscopic techniques. It was then used for the adsorption of the CVD in a batch system. This process was found to be highly dependent on the physicochemical parameters, such as the solution pH, the temperature, the contact time and the CVD initial concentration. The elimination of CVD by XHA reached 98.75%, and the process kinetic was of pseudo-second order. The results showed that the adsorption of the CVD dye is dominated by surface adsorption, resulting in the formation of a monomolecular CVD layer on the surface of XHA. The adsorption capacity was found to be 19.75 mg/g, according to the Langmuir model. The thermodynamic studies indicated that dye adsorption by XHA is spontaneous, endothermic and of a physisorption nature.

## Graphical abstract



**Keywords** Adsorption · Oil shale · Cristal violet dye · Adsorption isotherm · Thermodynamic parameters

✉ E. H. Chafyq  
elhassan7chafyq@gmail.com

Extended author information available on the last page of the article

## Introduction

The consequences of water pollution are mainly due to the discharge of untreated or partially treated effluents from various dye industries or wastewater treatment plants [1, 2].

Dyes are used in several industrial applications, such as textile, paper, leather, food, cosmetic and clinical products [3]. The crystal violet dye (CVD), which is a tri-phenyl-methane [4], is a member of the organic dye family that has been detected at higher concentrations in hospital and industrial effluents than concentrations typically found in surface, groundwater sources and wastewater [5, 6].

CVD is known to be carcinogenic and mutagenic, but it is still widely used in commercial textile operations, biological staining for histological tissues and Gram's method of identified bacteria (gram-positive and gram-negative) [7]. The dye can be impregnated with harmful amounts through the skin and cause skin irritation and digestive tract irritation [8]. Consequently, they present a serious concern for the environment and health [9]. For this reason, their removal from aqueous solutions is mandatory in terms of environmental and health protections [10, 11].

Several treatment processes have been used for decontamination of organic and inorganic water pollutants [12, 13], including oxidation processes [14], biotic treatment [15], membrane separation [16], conventional coagulation/flocculation and adsorption [17, 18]. The dyes are often hydrophilic and have a low affinity for the biomass and therefore biological treatment is often ineffective [19]. Adsorption was strongly adopted as a simple, low-cost and effective technology among the many treatment processes previously cited [20, 21].

Activated carbon is most commonly used to reduce color by adsorption. However, this material is only effective in some categories of dyes [22], among which the CVD [23], but their high cost and their loss during the regeneration restrict their application [24, 25]. For this reason, a large number of studies have been carried out to develop alternative and more economical adsorbents to remove the CVD.

The material elaborated from layer X of oil shales of the Timahdit region in the North of Morocco (XHA) is one of the common low-cost natural adsorbents [26]. The material presents a high active surface, large pore volume and good performance [27, 28].

The choice of oil shales-based materials as adsorbents seems to be interesting and efficient because of their functional sites that are related to the arrangement of the mineral and organic components within their structure. This confers on them some chemical properties leading to their strong affinity for organic contamination by the CVD [1, 29].

Also, the choice of oil shale is due to the fact that the majority of studies have focused on the energy exploitation

of Moroccan oil shale. M. Ziyad et al. have demonstrated non-isothermal kinetics of  $H_2S$  and  $H_2$  production from Timahdit oil shale [30], M. Halim et al. studied the characterization of the kerogen in the Timahdit oil shale (Y layer) based on a multistage degradation with alkaline permanganate [31] and A. Aboulkas and K. El Harfi studied the kinetics and mechanisms of thermal decomposition of Moroccan oil shale of Tarfaya kerogen [32].

On the contrary, our study is interested in the valorization of these non-exploitable oil shale in the field of environmental protection by preparing a new adsorbent.

This paper aims to study the feasibility of CVD adsorption using a phosphoric acid-activated adsorbent material (XHA). [33]. The XHA characterization was effected by scanning electron microscopy (SEM) and Fourier transforms infrared spectroscopy (FTIR) [34]. The kinetic parameters of the adsorption process by pseudo-first-order and pseudo-second-order models were evaluated. The efficiency of interactions between the CVD and XHA was evaluated and compared using the Langmuir and Freundlich adsorption isotherms. Additionally, a comparison of the thermodynamic parameters of the removal of the CVD by XHA was also made [35].

## Materials and methods

### Chemicals and instruments

The XHA adsorbent, with a particle size of less than 80  $\mu m$ , was elaborated from oil shale deposits from the layer X of the Timahdit region in Morocco. The samples were provided by the National Office of Petroleum Research and Exploitation (ONAREP) [28]. Phosphoric acid ( $H_3PO_4$ ) (30–70%), hydrochloric acid (HCl) (1M) and distilled water were used for chemical preparations and dilutions. The CVD (molecular formula  $C_{25}H_{30}N_3Cl$ , MW 407.99,  $\lambda_{max} = 591$  nm) was purchased from Sigma-Aldrich.

The mass of the samples was measured by the Nimbus® Analytical Balances (NBL 214i). The pH, the temperature and the conductivity were determined by a pH meter of WTW 522 type. The rotational speed was identified by the heated magnetic stirrer RT2 Basic (Thermo Scientific™), and the absorbance of the solution was measured using a UV–Visible spectrophotometer (Thermo Scientific Multi-skan<sup>FC</sup>) [36].

### Preparation of the CVD solution

A stock solution of CVD was prepared by precisely dissolving the CVD in distilled water at a concentration of 10 mg/L. The solutions for experiments were prepared by dilution,

and the pH was adjusted with 0.1 M HCl or 0.1 M NaOH solutions.

## Preparation of XHA

The mineralogical composition of the oil shales from layer X, used in this study, is illustrated in Table 1.

The raw rocks were crushed, ground and decarbonated using concentrated HCl (6 N) until the disappearance of CO<sub>2</sub> release by mixing 40 g of the sample (X) with 160 mL of 6 N HCl under continuous stirring (4 h). After filtration, the residue was washed with distilled water until it was exempt from chloride ions and then dried in the oven at 110 °C. The resulting product, labeled XH, was crushed and sieved to a particle size of 0.08 mm [38].

The chemical activation process of the obtained material consists of immersing the precursor XH in the chemical activating agent, 30–70% H<sub>3</sub>PO<sub>4</sub>. The mixture was introduced in the furnace previously preheated to predetermine temperature (250–450 °C) and kept at this temperature for 4 h under air. The excess acid was eliminated with distilled water using a Soxhlet extractor. The resulting product (XHA) was dehydrated in an oven at 110 °C and then sieved [39].

## Characterization

The FTIR spectral analysis of the samples was carried out using an IR Affinity-1S spectrometer in the wavenumber range from 500 to 4000 cm<sup>-1</sup> with a spectral resolution of 4 cm<sup>-1</sup> [40]. The surface morphology was studied using a JEOL JSM-IT200 SEM with voltages between 10 to 20 kV and magnification of 2000 to 4000 [41, 42].

## Batch adsorption studies

The adsorption kinetic of CVD onto XHA was conducted at room temperature in a batch system [43]. A liter of CVD stock solution, with an initial concentration of 10 mg/L, was prepared and poured into a series of beakers each containing 50 ml of solution.

During the adsorption experiment, 0.01 g of XHA was added to 0.05 L of the CVD solution with an initial

concentration between 5 and 300 mg/L. The batch reactor was stirred at a rotation speed of 125 rpm, and the reaction temperature was 293, 303, 313 and 333 K. Subsequently, 1 mL of the sample was taken at preset times (5–240 min) and the solid was separated from the solution by filtration using a 0.45 μm membrane. The values of the initial and equilibrium concentrations of the CVD were determined using a Thermo Scientific Multiskan<sup>FC</sup> spectrophotometer [44].

The percentage removal of the CVD was determined by calculation of the difference between its initial ( $C_i$  in mg/L) and final ( $C_f$  in mg/L) concentrations, using Eq. (1) [45]:

$$\%R = \frac{(C_i - C_f) * 100}{C_i} \quad (1)$$

The adsorption capacity ( $q_t$ ) was calculated using Eq. (2) [46]:

$$q(t) = \frac{(C_0 - C_t) * V}{m} \quad (2)$$

where  $q(t)$  is the amount of CVD adsorbed at time  $t$  (mg/g),  $C_0$  and  $C_t$  are the initial and time CVD concentrations (mg/L), respectively,  $V$  the volume of CVD solution (L) and  $m$  is the mass of adsorbent (g).

## Kinetic and equilibrium models

The pseudo-first-order and pseudo-second-order kinetic models were used for the analysis of the kinetic data [1, 47]. The equilibrium data were evaluated by applying Freundlich and Langmuir adsorption models, which models and equations are as follows [48]:

Pseudo-first order

$$\ln(Q_e - Q_t) = \ln(Q_e) - k_1 t \quad (3)$$

Pseudo-second order

$$\frac{t}{Q_t} = \frac{1}{k_2 Q_e^2} + \frac{t}{Q_e} \quad (4)$$

where  $Q_e$  and  $Q_t$  (mg/g) are the equilibrium and time  $t$  adsorption capacities of CVD on the adsorbent, respectively,  $k_1$  (min<sup>-1</sup>) the rate constant of the pseudo-first-order model and  $k_2$  (g/mg.min) the pseudo-second-order rate constant.

Langmuir isotherm model:

$$Q_e = \frac{Q_m K I C_e}{1 + K I C_e} \text{ Nonlinear form} \quad (5)$$

Freundlich isotherm model:

$$Q_e = k_f C_e^{1/n} \text{ Nonlinear form} \quad (6)$$

**Table 1** Mineralogical composition of (layer X) of the Timahdit region [27, 37]

Constituent	Percentage in weight
Calcite	15.6
Dolomite	13.8
Silica	23.7
Clay	26.9
Organic matter	20.0

where  $Q_e$  and  $Q_m$  (mg/g) represent the equilibrium and the maximum adsorption capacities, respectively,  $C_e$  (mg/L) is the equilibrium CVD concentration,  $K_L$  (L/mg) is the Langmuir constant that gives an indication of the adsorption strength of the adsorbate on the surface of the adsorbent, and  $K_F$  (mg/g) and  $n$  are Freundlich constants.

## Results and discussion

### Surface morphology

The SEM micrograph of XHA (Fig. 1a) shows that the particles exhibit a considerable number of heterogeneous pores, indicating that the adsorbent morphology has been altered by the chemical activation with  $H_3PO_4$  [49, 50]. This porous nature of XHA can facilitate the diffusion and penetration of CVD molecules into the internal surface of the XHA. After CVD adsorption, a remarkable change in the surface of XHA, which becomes saturated by CVD molecules, is noticed (Fig. 1b). Consequently, the efficiency of the adsorption phenomenon on XHA has been promoted [51, 52].

### FTIR analysis

The FTIR spectra of XHA before and after adsorption of CVD are shown in Fig. 2. The spectrum of XHA before adsorption presents a lower intensity for the peak at  $3434\text{ cm}^{-1}$ , which is attributed to the hydroxyl ( $-OH$ ) stretching vibration [53]. These groups belong to the desiccant effects of the acid treatment. After adsorption, the

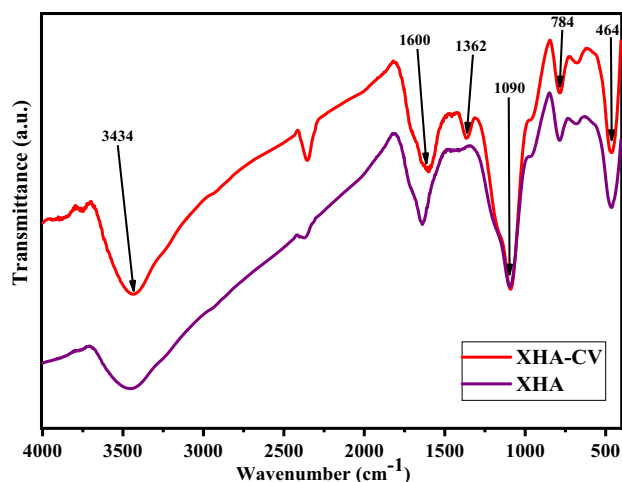


Fig. 2 FTIR spectrum of XHA before and after adsorption of CVD

intensities of this peak increased due to the functional O–H and N–H symmetric stretching vibrations in the CVD [54].

The intensity of the peak at  $1600\text{ cm}^{-1}$ , which corresponds to the presence of organic matter in XHA, increased after adsorption due to the presence of carbonyl group ( $C=O$ ) [55].

The peak centered around  $1090\text{ cm}^{-1}$  is indicative of the possible attributions: C–C elongation (aliphatic and aromatic alkanes) and C–O elongations. It could also be due to the Si–O groups. The increased intensity of this peak after adsorption is caused by the C–N elongations [56].

The new peak at  $1362\text{ cm}^{-1}$ , which appeared after adsorption, may be attributed to the stretching of C–H and C–N groups. It characterizes the possible involvement of these

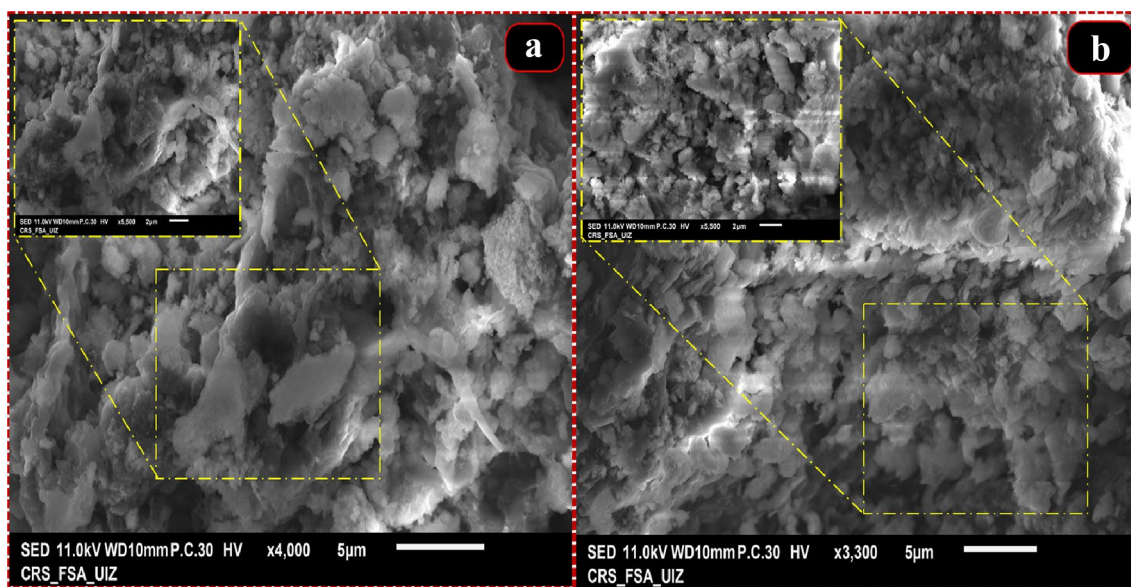


Fig. 1 SEM micrographs of XHA (a) and XHA-CVD (b) before and after adsorption

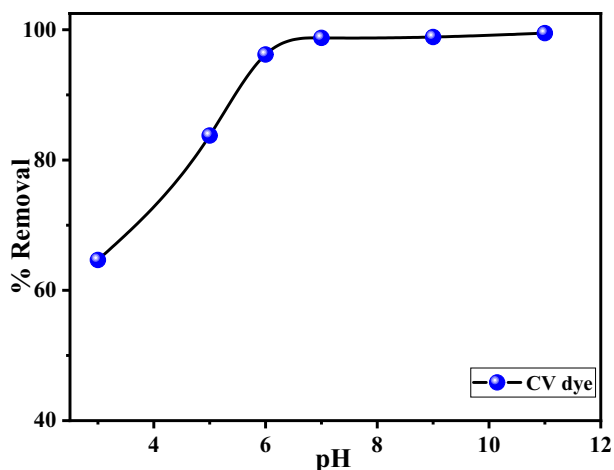


Fig. 3 Effect of initial pH on CVD adsorption on XHA

functional groups in the adsorption process of the CVD on the XHA surface [57].

## Adsorption study

### Effect of the pH

The effect of the pH, in the 3.0–11.0 range, on the adsorption of CVD by XHA is shown in Fig. 3. The percentage of CVD removed by the solid material increased from 71.22 to 98.89% when the solution pH was moved from 3.0 to 9.0 and remained constant beyond pH 9.0. Thereby, the CVD adsorption onto XHA is improved in the alkaline range because the interaction of the cationic dye with the negatively charged adsorption sites on the surface of XHA is enhanced. The leveling out of adsorption beyond pH 9.0 may be explained by the saturation of the surface sites of XHA and the increased concentration of hydroxyl ions in the solution that hinders the ion exchange between XHA and CVD [58]. The pH 9 value was used for the remainder of this study.

### The effect of contact time on adsorption

The effect of contact time on the adsorption of CVD by XHA for up to 240 min is illustrated in Fig. 4. The rapid increase in the percentage of removed CVD during the first 15 min may be explained by the availability of free active sites on the XHA surface [59]. These active sites become saturated after 120 min, and the adsorption reaches its maximum with CVD removal percentages of 98% and 99.47% at 120 and 240 min, respectively [60].

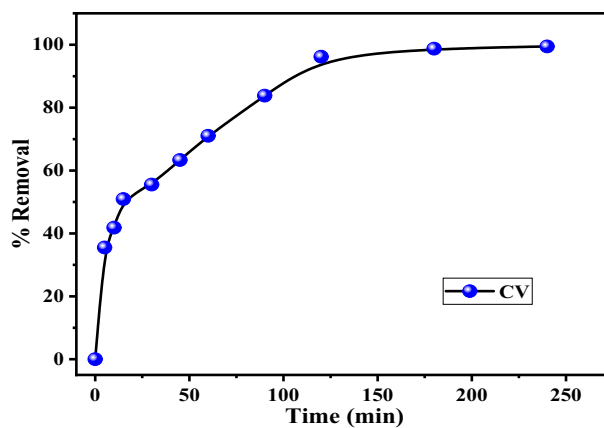


Fig. 4 Effect of contact time on CVD adsorption onto XHA

### Adsorption kinetic

The kinetic parameters obtained from both models for the adsorption of CVD on XHA are given in Table 2 and Figs. 5 and 6. The pseudo-first-order and pseudo-second-order models were used to test the adsorption kinetic data [61]. The pseudo-second-order model presents better fit for the experimental results, with a correlation coefficient ( $R^2$ ) of 0.990, compared to the pseudo-first-order model ( $R^2 = 0.946$ ). Moreover, the calculated equilibrium quantity ( $Q_{e_2} = 21.673$  mg/g) is closer to the experimental value ( $Q_{e_{exp}} = 19.89$  mg/g) for this model compared to the pseudo-first-order model ( $Q_{e_1} = 14.604$  mg/g).

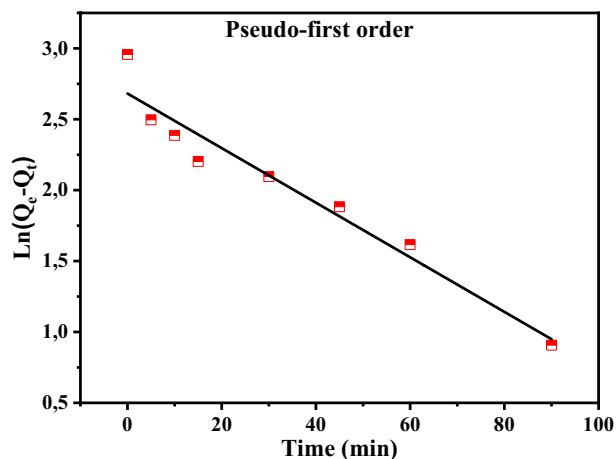
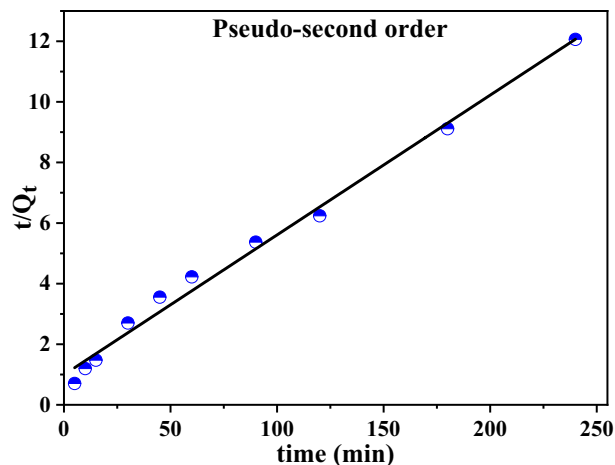
### Effect of initial concentration and adsorption isotherm

The results of the effect of CVD initial concentration on the CVD adsorption on XHA, in the 5–300 mg/L range, are presented in Fig. 7a. The amount adsorbed increases as a function of the equilibrium concentration until saturation, with a maximum adsorbed quantity of 55.84 mg/g. As the CVD concentration increases, it uses the free sites on the solid surface to adsorb before reaching saturation, as indicated by a plateau on the curve [62]. This phenomenon usually occurs when the interaction between the surface of the adsorbent and the solute is higher than that between the solvent and the solute [63].

Adsorption isotherm experiments were performed at different temperatures of 293, 303, 313 and 323 K with initial CVD concentrations in the 5.0–300 mg/L range and the adsorbent dose ranging from 125 to 1000 mg/L (Fig. 7 b). The calculated adsorption isotherm parameters (Table 3) indicate that the Langmuir model can better describe the CVD adsorption ( $R^2 = 0.9807$ ) than the Freundlich model ( $R^2 = 0.9299$ ). Thus, the CVD adsorption on XHA may be

**Table 2** Kinetic parameters for CVD adsorption on XHA

	$Q_{e,exp}$ (mg/g)	Pseudo-first order			Pseudo-second order		
		$R^2$	$Q_{e,1}$ (mg/g)	$k_1$ ( $\text{min}^{-1}$ )	$R^2$	$Q_{e,2}$ (mg/g)	$k_2$ (g/mg·min)
XHA	19.89	0.946	14.604	0.01924	0.990	21.673	$2.14 \times 10^{-3}$

**Fig. 5** Pseudo-first-order kinetic model for the CVD adsorption by XHA**Fig. 6** Pseudo-second-order kinetic model for the CVD adsorption by XHA

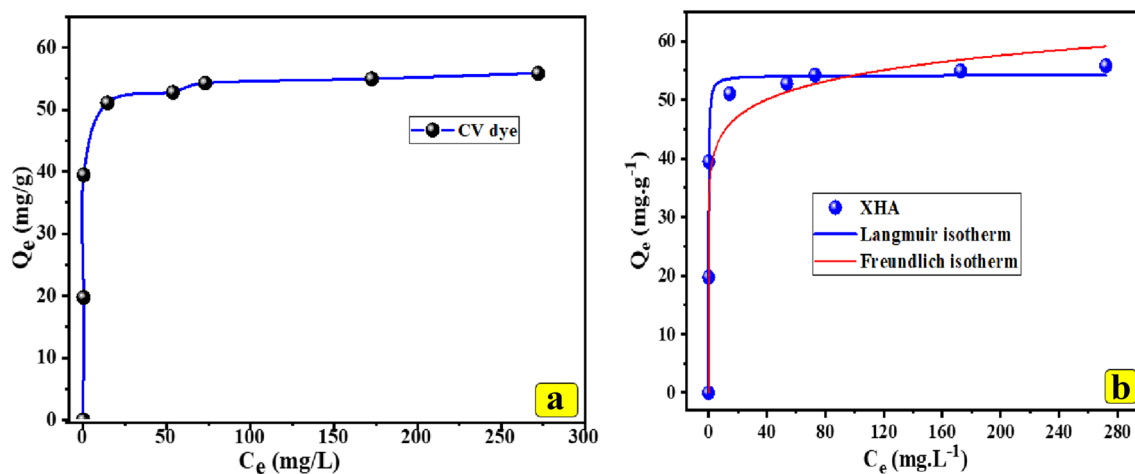
well determined by monolayer chemical adsorption with a maximum adsorbed quantity of 54.20 mg/g [64].

### Comparison of the XHA with other adsorbents

The different adsorbents reported in the literature regarding the removal of CVD by different methods are shown in Table 4. Our adsorbent (XHA) presents a better ability to remove CVD than most of these adsorbents.

### Thermodynamic parameters

The thermodynamic study was realized by varying the solution temperature from 20 to 50 °C. The CVD adsorption capacity increases with increasing temperature (Fig. 8 a) [71]. The thermodynamic parameters, such as free energy ( $\Delta G^\circ$ ), enthalpy ( $\Delta H^\circ$ ) and entropy ( $\Delta S^\circ$ ), were

**Fig. 7** (a) Effect of initial concentration of CVD on adsorption efficiency, (b) adsorption isotherm of nonlinear model for CVD adsorption on XHA

**Table 3** CVD adsorption parameters on XHA according to the Langmuir and Freundlich nonlinear model

Adsorbent	$Q_{\text{exp}}$ (mg/g)	Langmuir			Freundlich		
		$Q_{\text{max}}$ (mg/g)	$K_L$ (L·mg <sup>-1</sup> )	$R^2$	$n_f$	$K_F$ (mg·g <sup>-1</sup> )	$R^2$
XHA	45.26	54.2001	6.5116	0.9807	11.5045	36.3301	0.9299

**Table 4** Comparison of adsorption capacity of CVD by XHA with some other adsorbents

Adsorbents	$Q_{\text{max}}$ (mg/g)	References
Modified bambusa tulda	20.84	[65]
Agro-waste derived activated carbon	7.5717	[66]
Lignin-rich isolate from Elephant grass	24.99	[67]
TLAC/Chitosan composite	2.37	[54]
CO <sub>2</sub> plasma-treated PVDF membrane	3.84	[68]
Pumice stone	6.99	[69]
Moroccan pyrophyllite	9.58	[70]
XHA	54.20	present study

calculated from the Van't Hoff equation using Eqs. (7) and (8) and are given in Table 5 [72].

$$\Delta G^\circ = -RTL \ln K_d \quad (7)$$

$$\ln K_d = \frac{\Delta S^\circ}{R} - \frac{\Delta H^\circ}{RT} \quad (8)$$

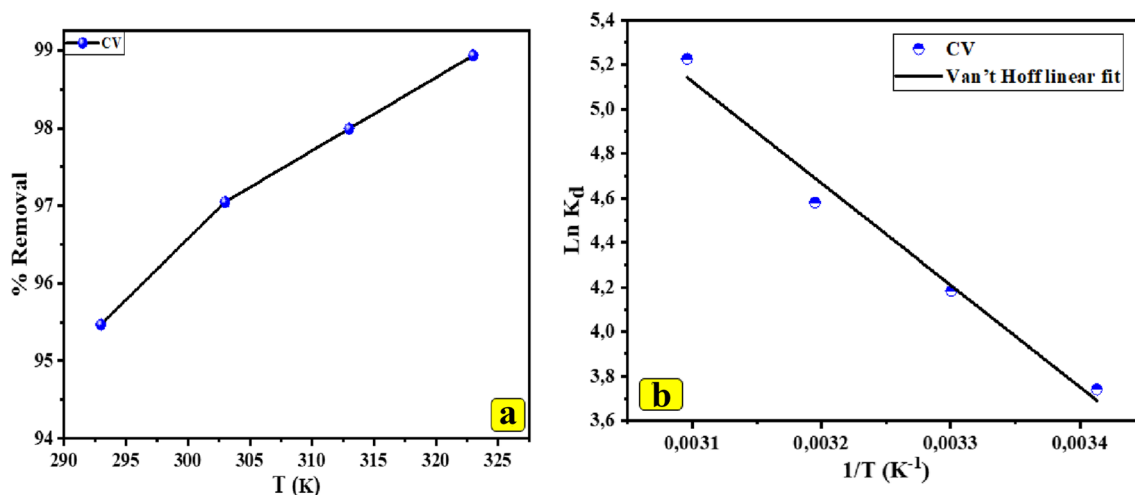
where  $R$  is the constant of perfect gases (8.314 J·mol<sup>-1</sup>·K<sup>-1</sup>),  $T$  is the absolute solution temperature (K) and  $K_d$  is the partition coefficient.

The  $\Delta H^\circ$  and  $\Delta S^\circ$  parameters are calculated using the linear regression analysis of the van't Hoff equation:  $\ln K_d = f(1/T)$  (Fig. 8 b). The adsorption process

is spontaneous ( $\Delta^\circ < 0$ ), endothermic ( $\Delta H^\circ = 38.014$  kJ/mol) and presents an increasing randomness between the solid–solution interfaces ( $\Delta S^\circ = 160.42$  J/mol/K) [73]. The negative values of  $\Delta G^\circ$  which are within 20 and 0 kJ/mol range show that the mechanism is dominated by the physical reaction. It is also noted that this energy increases with temperature, indicating that the CVD adsorption on XHA is more favorable at lower temperatures [74, 75].

## Conclusion

This study shows that adsorbent materials, prepared from Moroccan oil shales of Timahdit (layer X), present efficient materials for the removal of CVD from aqueous solutions. The results indicate that the adsorption is also influenced by experimental factors, such as contact time, initial CVD concentration, pH value and temperature. The adsorption isotherm of XHA-CVD reveals a monolayer process, which is better described by the Langmuir model with a maximum adsorption capacity of 54.20 mg/g. The kinetic study shows that the adsorption process obeys the pseudo-second-order model, which implies it depends on both time and concentration. The thermodynamic parameters obtained indicate the CVD adsorption on XHA is spontaneous, endothermic and governed by a physisorption process.

**Fig. 8** (a) Effect of temperature on the CVD adsorption on XHA and (b) effect of temperature on the distribution constant of the adsorption

**Table 5** Thermodynamic parameters for adsorption of CVD on XHA adsorbent

	$\Delta H^\circ$ (KJ/mol)	$\Delta S^\circ$ (J/mol/K)	$\Delta G^\circ$ (KJ/mol)			
			293 K	303 K	313 K	323 K
XHA	38.014	160.42	-9.11	-10.53	-11.91	-14.02

Moreover, the preparation of XHA was simple, inexpensive and environment-friendly. Thus, the application of XHA in the removal of CVD from wastewater and groundwater presents great development prospects. It can be concluded that the application of modified Moroccan oil shales for removing CVD from aqueous solutions is highly feasible.

## References

- K. Legrouiri, E. Khouya, M. Ezzine, H. Hannache, R. Denoyel, R. Pallier, R. Naslain, *J. Hazard. Mater.* **118**, 259 (2005)
- A. Khanmohammadi, A. Jalili-Ghazizadeh, P. Hashemi, A. Afkhami, F. Arduini, H. Bagheri, *J. Iran. Chem. Soc.* **17**, 2429 (2020)
- N. Hareesha, J.G. Manjunatha, *J. Iran. Chem. Soc.* **17**, 1507 (2020)
- G. Vyavahare, P. Jadhav, J. Jadhav, R. Patil, C. Aware, D. Patil, A. Gophane, Y.-H. Yang, R. Gurav, *J. Clean. Prod.* **207**, 296 (2019)
- T. Van Tran, T.-Q.T. Phan, D.T.C. Nguyen, T.T. Nguyen, D.H. Nguyen, D.-V.N. Vo, L.G. Bach, T.D. Nguyen, *Environ. Technol. Innov.* **20**, 101122 (2020)
- R. Mehrkhah, E.K. Goharshadi, M. Mohammadi, *J. Ind. Eng. Chem.* **101**, 334 (2021)
- H.T. Elbalkiny, A.M. Yehia, M.R. Safa'a, Y.S. Elsharty, *Microchem. J.* **145**, 90 (2019)
- A. Deb, M. Kanmani, A. Debnath, K.L. Bhowmik, B. Saha, *Ultrason. Sonochem.* **54**, 290 (2019)
- K. Tanji, M. Zouheir, Y. Naciri, H. Ahmoum, A. Hsini, O. Mertah, A. El Gaidoumi, J.A. Navio, M.C. Hidalgo, A. Kherbeche, *J. Iran. Chem. Soc.* **19**, 2779 (2022)
- R. Mehrkhah, E.K. Goharshadi, M.M. Ghafurian, M. Mohammadi, O. Mahian, *Sol. Energy* **224**, 440 (2021)
- N. Yazdanfar, M. Shamsipur, M. Ghambarian, *J. Iran. Chem. Soc.* **18**, 1433 (2021)
- K.S.D. Premarathna, A.U. Rajapaksha, B. Sarkar, E.E. Kwon, A. Bhatnagar, Y.S. Ok, M. Vithanage, *Chem. Eng. J.* **372**, 536 (2019)
- M. Karimi-Nazarabad, E.K. Goharshadi, R. Mehrkhah, M. Davardoostmanesh, *Sep. Purif. Technol.* **279**, 119788 (2021)
- E.M. Cuerda-Correa, M.F. Alexandre-Franco, C. Fernández-González, *Water* **12**, 102 (2020)
- C.X. Hiller, U. Hübner, S. Fajnorova, T. Schwartz, J.E. Drewes, *Sci. Total Environ.* **685**, 596 (2019)
- A. Mudhoo, A. Bhatnagar, M. Rantalankila, V. Srivastava, M. Sillanpää, *Chem. Eng. J.* **360**, 912 (2019)
- A. Hsini, A. Essekre, N. Aarab, M. Laabd, A. Ait-Addi, R. Lakmiri, A. Albourine, *Environ. Sci. Pollut. Res.* **27**, 15245 (2020)
- S.A. Bhat, F. Zafar, A.H. Mondal, A. Kareem, A.U. Mirza, S. Khan, A. Mohammad, Q.M. Haq, N. Nishat, *J. Iran. Chem. Soc.* **17**, 215 (2020)
- S. Zhao, Z. Bai, B. Wang, T. Tian, Z. Hu, *Sep. Purif. Technol.* **241**, 116633 (2020)
- S.S. Fiyadh, M.A. AlSaadi, W.Z. Jaafar, M.K. AlOmar, S.S. Fayaed, N.S. Mohd, L.S. Hin, A. El-Shafie, *J. Clean. Prod.* **230**, 783 (2019)
- S. Ganesan, M. Amirthalingam, P. Arivalagan, S. Govindan, S. Palanisamy, A.P. Lingassamy, V.K. Ponnusamy, *J. Environ. Manag.* **245**, 409 (2019)
- W. Xiao, Z.N. Garba, S. Sun, I. Lawan, L. Wang, M. Lin, Z. Yuan, *J. Clean. Prod.* **253**, 119989 (2020)
- Z. Falaki, H. Bashiri, *J. Iran. Chem. Soc.* **18**, 2689 (2021)
- Z. Liu, B. Ren, H. Ding, H. He, H. Deng, C. Zhao, P. Wang, D.D. Dionysiou, *Water Res.* **171**, 115456 (2020)
- S.O. Adio, M. Asif, A.-R.I. Mohammed, N. Baig, A.A. Al-Arfaj, T.A. Saleh, *Process Saf. Environ. Prot.* **121**, 254 (2019)
- A. Ghorbani-Choghamarani, P. Moradi, B. Tahmasbi, *J. Iran. Chem. Soc.* **16**, 511 (2019)
- E.H. Chafyq, K. Legrouiri, M. Oumam, S. Mansouri, M. Aghrouch, E.H. Khouya, H. Hannache, *Groundw. Sustain. Dev.* **12**, 100532 (2021)
- M. Oumam, A. Abourriche, S. Mansouri, M. Mouiya, A. Benhammou, Y. Abouliatim, Y. El Hafiane, H. Hannache, M. Birot, R. Pailler, *Oil Shale* **37**, 139 (2020)
- W. Li, X. Pang, C. Snape, B. Zhang, D. Zheng, X. Zhang, *Energy Fuels* **33**, 765 (2019)
- M. Ziyad, J.-P.P. Garnier, M. Halim, *Fuel* **65**, 715 (1986)
- A. Amblès, M. Halim, J.-C. Jacquesy, D. Vitorovic, M. Ziyad, *Fuel* **73**, 17 (1994)
- A. Aboulkas, K. El Harfi, *Oil Shale* **25**, 426 (2008)
- S. Ichcho, E. Khouya, S. Fakhri, M. Ezzine, H. Hannache, R. Pallier, R. Naslain, *J. Hazard. Mater.* **118**, 45 (2005)
- C. Gecgel, U.B. Simsek, B. Gozmen, M. Turabik, *J. Iran. Chem. Soc.* **16**, 1735 (2019)
- M. Karimi-Nazarabad, H. Azizi-Toupkanloo, *J. Iran. Chem. Soc.* **19**, 1527 (2022)
- N. Jalili-Jahani, B. Hemmateenejad, M. Shamsipur, *J. Iran. Chem. Soc.* **17**, 1173 (2020)
- S. Mansouri, H. Majdoubi, Y. Haddaji, Y. Tamraoui, M. El Achaby, B. Manoun, A. Abourriche, H. Hannache, M. Oumam, *Chem. Res. Chin. Univ.* **36**, 1339 (2020)
- A.K. Abourriche, M. Oumam, H. Hannache, M. Birot, Y. Abouliatim, A. Benhammou, Y. El Hafiane, A.M. Abourriche, R. Pailler, R. Naslain, *J. Supercrit. Fluid* **84**, 98 (2013)
- H. Khouya, K. Legrouiri, S. Fakhri, H. Hannache, *Nat. Preced.* **5**, 1 (2010)
- Y. Haddaji, H. Majdoubi, S. Mansouri, Y. Tamraoui, B. Manoun, M. Oumam, H. Hannache, *Mater. Chem. Phys.* **260**, 124147 (2021)
- Y. Naciri, A. Hsini, Z. Ajmal, A. Bouddouch, B. Bakiz, J.A. Navio, A. Albourine, J. Valmalette, M. Ezahri, A. Benhachemi, *J. Colloid Interface Sci. J.* **572**, 269 (2020)
- M. Shamsipur, A. Barati, A.A. Taherpour, M. Jamshidi, *J. Phys. Chem. Lett.* **9**, 4189 (2018)
- T.L. Palma, B. Vieira, J. Nunes, J.P. Lourenço, O.C. Monteiro, M.C. Costa, *J. Iran. Chem. Soc.* **17**, 2013 (2020)
- H. Hu, J. Liu, Z. Xu, L. Zhang, B. Cheng, W. Ho, *Appl. Surf. Sci.* **478**, 981 (2019)
- H. Mittal, A. Al-Alili, P.P. Morajkar, S.M. Alhassan, *J. Mol. Liq.* **323**, 115034 (2021)



46. H.-O. Chahinez, O. Abdelkader, Y. Leila, H.N. Tran, *Environ. Technol. Innov.* **19**, 100872 (2020)
47. Y. Naciri, A. Hsini, Z. Ajmal, J.A. Navío, B. Bakiz, A. Albourine, M. Ezahri, A. Benlhachemi, *Adv. Colloid Interface Sci.* **280**, 102160 (2020)
48. A. Hsini, Y. Naciri, M. Laabd, M. El Ouardi, Z. Ajmal, R. Lakhmiri, R. Boukherroub, A. Albourine, *J. Mol. Liq.* **316**, 113832 (2020)
49. Q. Han, J. Wang, B.A. Goodman, J. Xie, Z. Liu, *Powder Technol.* **366**, 239 (2020)
50. A. Maleki, V. Eskandarpour, *J. Iran. Chem. Soc.* **16**, 1459 (2019)
51. C. Du, Y. Song, S. Shi, B. Jiang, J. Yang, S. Xiao, *Sci. Total Environ.* **711**, 134662 (2020)
52. H. Sarvari, E.K. Goharshadi, S. Samiee, N. Ashraf, *Phys. Chem. Res.* **6**, 433 (2018)
53. A. Khorshidi, S. Ansari, S. Shariati, *J. Iran. Chem. Soc.* **19**, 3473 (2022)
54. H.J. Kumari, P. Krishnamoorthy, T.K. Arumugam, S. Radhakrishnan, D. Vasudevan, *Int. J. Biol. Macromol.* **96**, 324 (2017)
55. R. Fabryanty, C. Valencia, F.E. Soetaredjo, J.N. Putro, S.P. Santoso, A. Kurniawan, Y.-H. Ju, S. Ismadji, *J. Environ. Chem. Eng.* **5**, 5677 (2017)
56. K.N.A. Putri, A. Keereerak, W. Chinpa, *Int. J. Biol. Macromol.* **156**, 762 (2020)
57. M.R. Kulkarni, T. Revanth, A. Acharya, P. Bhat, *Resour. Technol.* **3**, 71 (2017)
58. A.I. Abd-Elhamid, M. Emran, M.H. El-Sadek, A.A. El-Shanshory, H.M.A. Soliman, M.A. Akl, M. Rashad, *Appl. Water Sci.* **10**, 1 (2020)
59. A.F.M. Streit, L.N. Côrtes, S.P. Druzian, M. Godinho, G.C. Collazzo, D. Perondi, G.L. Dotto, *Sci. Total Environ.* **660**, 277 (2019)
60. S. Mohanty, S. Moulick, S.K. Maji, *J. Water Process. Eng.* **37**, 101428 (2020)
61. N.S. Al-Kadhi, *Egypt. J. Aquat. Res.* **45**, 231 (2019)
62. H.M. Mashhoor, M. Eftekhari, N. Rezazadeh, M.K. Nazarabad, *Nanotechnol. Environ. Eng.* (2022). <https://doi.org/10.1007/s41204-022-00269-7>
63. Z. Li, L. Sellaoui, D. Franco, M.S. Netto, J. Georgin, G.L. Dotto, A. Bajahzar, H. Belmabrouk, A. Bonilla-Petriciolet, Q. Li, *Chem. Eng. J.* **389**, 124467 (2020)
64. X. Pang, L. Sellaoui, D. Franco, G.L. Dotto, J. Georgin, A. Bajahzar, H. Belmabrouk, A. Ben-Lamine, A. Bonilla-Petriciolet, Z. Li, *Chem. Eng. J.* **378**, 122101 (2019)
65. N. Laskar, U. Kumar, *KSCE J. Civ. Eng.* **22**, 2755 (2018)
66. E.E. Jasper, V.O. Ajibola, J.C. Onwuka, *Appl. Water Sci.* **10**, 1 (2020)
67. M.C. Menkiti, C.O. Aniagor, C.M. Agu, V.I. Ugonabo, *Water Conserv. Sci. Eng.* **3**, 33 (2018)
68. D.A. Gopakumar, V. Arumukhan, R.V. Gelamo, D. Pasquini, L.C. de Moraes, S. Rizal, D. Hermawan, A. Nzihou, H.P.S.A. Khalil, *Nanostruct. Nanoobject* **18**, 100268 (2019)
69. H. Shayesteh, A. Rahbar-Kelishami, R. Norouzbeigi, *Desalin. Water Treat.* **57**, 12822 (2016)
70. Y. Miyah, A. Lahrichi, M. Idrissi, S. Boujraf, H. Taouda, F. Zerrouq, *J. Assoc. Arab Univ. Basic Appl. Sci.* **23**, 20 (2017)
71. A. Djelad, A. Mokhtar, A. Khelifa, A. Bengueddach, M. Sassi, *Int. J. Biol. Macromol.* **139**, 944 (2019)
72. E.C. Lima, A.A. Gomes, H.N. Tran, *J. Mol. Liq.* **311**, 113315 (2020)
73. A. Mirza, R. Ahmad, *Groundw. Sustain. Dev.* **11**, 100373 (2020)
74. M. Karimi-Nazarabad, E.K. Goharshadi, H.-S. Sajjadizadeh, *J. Phys. Chem. C* **126**, 8199 (2022)
75. S.M. Yakout, M.R. Hassan, A.A. Abdeltawab, M.I. Aly, *J. Clean. Prod.* **234**, 124 (2019)

Springer Nature or its licensor holds exclusive rights to this article under a publishing agreement with the author(s) or other rightsholder(s); author self-archiving of the accepted manuscript version of this article is solely governed by the terms of such publishing agreement and applicable law.

## Authors and Affiliations

E. H. Chafyq<sup>1</sup>  · K. Legrouri<sup>1,2</sup> · M. Aghrouch<sup>4</sup> · M. Oumam<sup>1</sup> · S. Mansouri<sup>3</sup> · E. Khouya<sup>1,5</sup> · H. Hannache<sup>1,3</sup>

<sup>1</sup> LIMAT-Thermostructural Materials and Polymers Team, Faculty of Science Ben M'sick, University Hassan II of Casablanca, Boulevard Cdt Driss Harti, BP.7955, Ben M'sick, Casablanca, Morocco

<sup>2</sup> Higher Institute of Nursing Professions and Technics Health, ISPITS, Agadir, Morocco

<sup>3</sup> Materials Science and Nanoengineering Department, Mohamed VI Polytechnic University, Lot 660 Hay Moulay Rachid, 43150 Benguerir, Morocco

<sup>4</sup> Medical Analysis Laboratory, Regional Hospital Centre Hassan II, Agadir, Morocco

<sup>5</sup> Regional Center for Teaching and Formation Profession CRMEF- Souss Massa, Avenue My Abdallah BP. N° 106, Inzegane, Morocco